Inorganic Chemistry

pubs.acs.org/IC

Article

Group 11 *m*-Terphenyl Complexes Featuring Metallophilic Interactions

Yu Liu, Laurence J. Taylor, Stephen P. Argent, Jonathan McMaster, and Deborah L. Kays*

Cite This: *Inorg. Chem.* 2021, 60, 10114−10123

Read Online

ACCESS | Metrics & More | Article Recommendations | Supporting Information

ABSTRACT: A series of group 11 *m*-terphenyl complexes have been synthesized via a metathesis reaction from the iron(II) complexes $(2,6\text{-}Mes_2C_6H_3)_2Fe$ and $(2,6\text{-}Xyl_2C_6H_3)_2Fe$ (Mes = 2,4,6-$Me_3C_6H_2$; Xyl = 2,6-$Me_2C_6H_3$). $[2,6\text{-}Mes_2C_6H_3M]_2$ (**1**, M = Cu; **2**, M = Ag; **6**, M = Au) and $[2,6\text{-}Xyl_2C_6H_3M]_2$ (**3**, M = Cu; **4**, M = Ag) are dimeric in the solid state, although different geometries are observed depending on the ligand. These complexes feature short metal−metal distances in the expected range for metallophilic interactions. While **1**−**4** are readily isolated using this metathetical route, the gold complex **6** is unstable in solution at ambient temperatures and has only been obtained in low yield from the decomposition of $(2,6\text{-}Mes_2C_6H_3)Au{\cdot}SMe_2$ (**5**). NMR spectroscopic measurements, including diffusion-ordered spectroscopy, suggest that **1**−**4** remain dimeric in a benzene-d_6 solution. The metal−metal interactions have been examined computationally using the Quantum Theory of Atoms in Molecules and by an energy decomposition analysis employing natural orbitals for chemical valence.

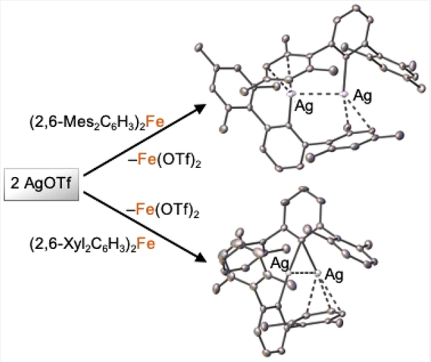

INTRODUCTION

Metallophilic interactions are a class of attractive metal−metal interactions that occur between formally closed-shell (d^{10} and s^2) or *pseudo*-closed-shell (d^8) metal atoms.[1,2] Metallophilic interactions are often described as correlation−dispersion interactions[1] and have been observed for a range of late transition metals.[1,2] They are particularly prominent for the group 11 metal(I) salts, and numerous examples of aurophilic (Au^I−Au^I),[3,4] argentophilic (Ag^I−Ag^I),[5] and cuprophilic (Cu^I−Cu^I)[6] interactions have been reported. While somewhat counterintuitive, given the expected large Coulombic repulsion between metal ions, these interactions have been proposed to play a role in supramolecular chemistry,[7−10] ion sensing,[11] luminescence,[8,12−14] and catalysis.[15−21] However, despite their importance, the exact nature and strength of these interactions is still debated.[1,3,4,22−27]

m-Terphenyls are a class of sterically bulky ligands that have been utilized repeatedly in the stabilization of low-coordinate main-group and transition-metal complexes.[28−32] They have proven to be useful in stabilizing metal−metal covalent bonds,[32−35] most notably the first example of a Cr−Cr quintuple bond.[36,37] Within the group 11 metals, most research has focused on copper(I) *m*-terphenyl complexes,[38−50] with less work on the related silver(I)[45,51] and gold(I)[52,53] complexes. Several of the copper(I) complexes feature short Cu(I)···Cu(I) contacts.[38,43,46,47] However, none of these reports discuss metallophilic interactions, and these close contacts are assessed as nonbonding; this may reflect the controversial nature of cuprophilic interactions at the time of the original publication.[6] To the best of our knowledge, no investigations have been carried out on the use of the *m*-terphenyl scaffold to support metallophilic interactions. Herein, we report the synthesis and characterization of several group 11 *m*-terphenyl complexes via a metathesis route from $(2,6\text{-}Mes_2C_6H_3)_2Fe$ or $(2,6\text{-}Xyl_2C_6H_3)_2Fe$ (Mes = 2,4,6-$Me_2C_6H_2$; Xyl = 2,6-$Me_2C_6H_3$), which feature close M···M contacts in the solid state. Diffusion-ordered spectroscopy (DOSY) is used to determine the aggregation state in solution, and the intramolecular interactions are analyzed computationally using the Quantum Theory of Atoms in Molecules (QTAIM)[54,55] and an energy decomposition analysis employing natural orbitals for chemical valence (EDA-NOCV).[56−59]

RESULTS AND DISCUSSION

Synthesis and Characterization. The reaction between the two-coordinate iron(II) *m*-terphenyl complexes $(2,6\text{-}Mes_2C_6H_3)_2Fe$[30] or $(2,6\text{-}Xyl_2C_6H_3)_2Fe$[60] and the appropriate group 11 triflate salt ($[CF_3SO_3Cu]_2{\cdot}C_6H_6$ or CF_3SO_3Ag) in a diethyl ether solution resulted in the formation of dimeric group 11 *m*-terphenyl complexes **1**−**4** (Scheme 1). This methodology is distinctly different from previous work in this field, which exclusively used organolithium or Grignard reagents in the synthesis of group 11 *m*-terphenyl complexes.[38−53] After recrystallization from isohexane or diethyl

Received: December 14, 2020
Published: July 1, 2021

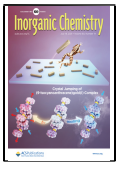

https://doi.org/10.1021/acs.inorgchem.0c03623
Inorg. Chem. 2021, 60, 10114−10123

Scheme 1. Synthesis of Group 11 *m*-Terphenyl Complexes 1−4[a]

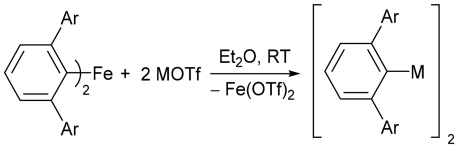

1: M = Cu; Ar = Mes
2: M = Ag; Ar = Mes
3: M = Cu; Ar = Xyl
4: M = Ag; Ar = Xyl

[a]Ar = Mes or Xyl. OTf = triflate, $CF_3SO_3^-$. MOTf = 0.5-$[CF_3SO_3Cu]_2{\cdot}C_6H_6$ or CF_3SO_3Ag. RT = room temperature.

ether at −30 °C, compounds **1**−**4** were obtained in moderate-to-good yields (44−87%) and characterized by NMR spectroscopy (including DOSY measurements), mass spectrometry, elemental analysis, and X-ray crystallography. Species **1** was reported previously by Niemeyer via the reaction of [2,6-$Mes_2C_6H_3Li$] with CuO*t*Bu, albeit in lower yield (55% vs 68%).[43]

Single-crystal X-ray diffraction measurements confirm complexes **1**−**4** to be dimeric in the solid state. The conformation varies depending on the identity of the flanking aryl group, with **1** and **2** adopting structures featuring terminal coordination of both ligands (terminal geometry; Figure 1), while **3** and **4** adopt structures with one bridging ligand and one terminal ligand (bridged geometry; Figure 2).

Compounds **1**−**4** show short M···M distances (M = Cu, Ag), within the expected range for cuprophilic/argentophilic interactions,[5,6] as well as apparent π−arene interactions to C atoms on the flanking aryl rings (Table 1). The structure of **1** is analogous to the one published by Niemeyer in 1998, albeit

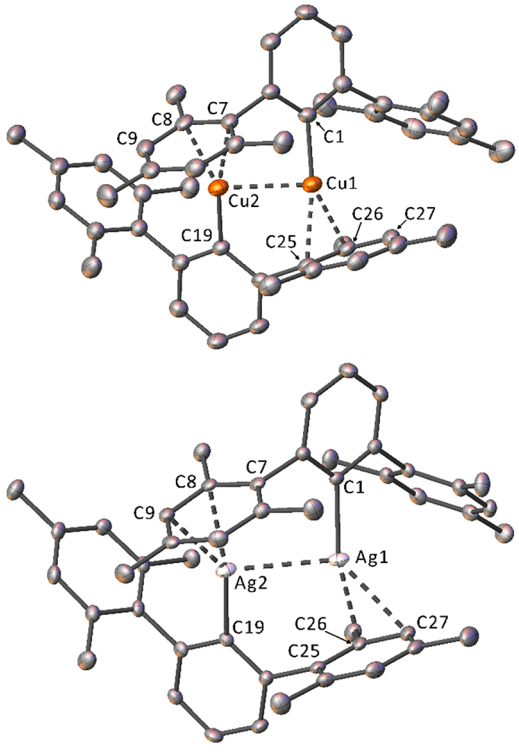

Figure 1. Crystal structures of **1** (top) and **2** (bottom) with displacement ellipsoids set to 50%. H atoms omitted for clarity.

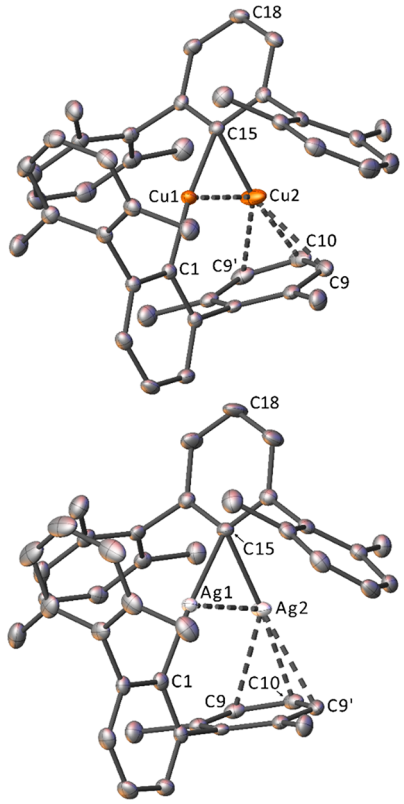

Figure 2. Crystal structures of **3** (top) and **4** (bottom) with displacement ellipsoids set to 50%. H atoms and additional molecules in the asymmetric unit (**4**) omitted for clarity. Symmetry operation for **3** (′): $+x, 1-y, +z$. Symmetry operation for **4** (′): $+x, {}^1/_2-y, +z$.

with a reduced Cu···Cu distance [2.5808(7) Å, previously reported as 2.5953(12) Å].[43] Complex **2** appears to be the silver analogue of **1**, and no other terphenyl complexes featuring two Ag centers have been published.

Compound **2** can be compared to $[(ITr)Ag_2]_2^{2+}$ (ITr = $[(HCNCPh_3)_2C:]$), which exists as a dimer involving aryl−Ag(I) η^2-interactions.[61] However, $[(ITr)Ag_2]_2^{2+}$ does not feature close contact between the Ag centers [Ag···Ag = 5.0708(6) Å].[61] Complexes **1** and **2** also bear structural similarities to the M(I) dimers [Ar′MMAr′] [Ar′ = 2,6-(2,6-*i*PrC_6H_3)C_6H_3; M = Cr, Fe, Co] published by Power and coworkers.[36,62] [Ar′CrCrAr′] features a short Cr−Cr quintuple bond [1.8351(4) Å],[36] while the iron and cobalt analogues feature weaker metal−metal interactions.[62] However, these species are open-shell, and thus the nature of the metal−metal interactions is quite different from that of the formally closed-shell interactions in **1** and **2**.

The bridged structure of **3** can be compared to $[(Me_2S)_2Cu(\mu\text{-}C_6H_2\text{-}2,4,6\text{-}Ph_3)Cu(C_6H_2\text{-}2,4,6\text{-}Ph_3)]$,[38] which features two terphenyl ligands, one bridging and one terminal, coordinating two Cu atoms in a manner similar to that of **3**. The Cu···Cu distance in $[(Me_2S)_2Cu(\mu\text{-}C_6H_2\text{-}2,4,6\text{-}Ph_3)Cu(C_6H_2\text{-}2,4,6\text{-}Ph_3)]$ [2.443(1) Å] is longer than that in **3** [2.4112(5) Å].[38] Another related complex, $[Li(THF)_4][2,6\text{-}Mes_2C_6H_3(CuI)_2]$,[46] features two CuI moieties bound to the same *ipso*-C of a *m*-terphenyl ligand. $[2,6\text{-}Mes_2C_6H_3(CuI)_2]^-$ features a very short Cu···Cu distance [2.391(3) Å], although the authors do not attribute this to a cuprophilic interaction.[46] Compound **4** is the silver analogue of **3**, and we can find no directly comparable terphenyl complexes in the literature. It

https://doi.org/10.1021/acs.inorgchem.0c03623
Inorg. Chem. 2021, 60, 10114−10123

Table 1. Selected Bond Lengths (Å) and Angles (deg) for Compounds 1−4 and 6

		1				**2**	
C1−Cu1	1.920(3)	C25···Cu1	2.275(3)	C1−Ag1	2.092(3)	C25···Ag1	2.843(3)
C19−Cu2	1.919(3)	C26···Cu1	2.126(3)	C19−Ag2	2.090(3)	C26···Ag1	2.380(2)
Cu1···Cu2	2.5808(7)	C27···Cu1	2.600(3)	Ag1···Ag2	2.8633(4)	C27···Ag1	2.486(3)
C7···Cu2	2.215(3)	C1−Cu1···Cu2	86.9(1)	C7···Ag2	2.778(3)	C1−Ag1···Ag2	91.12(7)
C8···Cu2	2.157(3)	C19−Cu2···Cu1	87.5(1)	C8···Ag2	2.372(2)	C19−Ag2···Ag1	93.05(7)
C9···Cu2	2.615(3)			C9···Ag2	2.572(2)		
		3				**6**	
C1−Cu1	1.937(3)	C10···Cu2	2.163(3)	C1−Au1	2.01(1)	C25···Au1	2.96(1)
C15−Cu1	2.002(3)	C1−Cu1−C15	170.99(14)	C19−Au2	1.99(1)	C26···Au1	2.38(1)
C15−Cu2	2.012(3)	Cu1−C15−Cu2	73.85(11)	Au1···Au2	3.2312(6)	C27···Au1	2.37(1)
Cu1···Cu2	2.4112(5)	Cu1−C15···C18	166.30(16)	C7···Au2	2.94(1)	C1−Au1···Au2	93.6(3)
C9···Cu2	2.331(2)			C8···Au2	2.37(1)	C19−Au2···Au1	95.0(3)
				C9···Au2	2.348(9)		
			4[a]				
C1−Ag1	2.106(3) [2.115(3)] {2.123(3)}			C10···Ag2	2.419(3) [2.408(3)] {2.409(3)}		
C15−Ag1	2.236(3) [2.219(3)] {2.239(3)}			C1−Ag1−C15	174.16(12) [172.98(12)] {172.14(12)}		
C15−Ag2	2.238(3) [2.224(3)] {2.232(3)}			Ag1−C15−Ag2	73.3(1) [73.90(11)] {73.12(9)}		
Ag1···Ag2	2.6706(3) [2.6709(3)] {2.6630(4)}			Ag1−C15···C18	150.96(16) [154.87(16)] {156.07(16)}		
C9···Ag2	2.652(3) [2.634(3)] {2.626(3)}						

[a]Measurements for the second and third molecules in the asymmetric unit are given in square and curly brackets, respectively.

should be noted that the reaction of $[2,6\text{-}Mes_2C_6H_3Li]_2$ with AgOCN affords the mononuclear argentate salt $[(2,6\text{-}Mes_2C_6H_3)_2Ag][Li(THF)_4]$[51] rather than a bimetallic species like **2** or **4**. Thus, the metathesis route reported here is the only known method for the syntheses of bimetallic silver *m*-terphenyl complexes.

We also note, for comparison with **1**−**4**, the crystal structures of the terphenyl complexes $2,4,6\text{-}Ph_3C_6H_2M$ (M = Cu, Ag) published in 1988.[63] These were originally reported as monocoordinated copper(I) and silver(I) aryl species, but later work called these results into question, suggesting that the crystals consisted mostly or entirely of $2,4,6\text{-}Ph_3C_6H_2Br$.[64] No other examples of monocoordinated copper(I) or silver(I) aryls have been reported to date.

NMR spectroscopic measurements reveal one set of signals for both terphenyl ligands in the ^1H and $^{13}C\{^1H\}$ NMR spectra of **1**−**4**. However, the *ipso*-C $^{13}C\{^1H\}$ NMR signals of complexes **2** and **4** appear as pseudotriplets (Figures S4 and S8). Furthermore, DOSY measurements on **1**−**4** show the presence of only one species in solution, with computed hydrodynamic radii more consistent with dimers than monomers. We therefore conclude that **1**−**4** remain as dimers in a benzene-d_6 solution but with fluxional structures because all ligands appear to be magnetically equivalent on the NMR time scale. The pseudotriplets in the $^{13}C\{^1H\}$ NMR spectra of **2** and **4** can be rationalized as ^1J coupling to two Ag atoms, which appear magnetically equivalent due to fast exchange. The difference in the coupling constants of the two silver isotopes (^{107}Ag and ^{109}Ag, both $I = {}^1/_2$) is likely too small to resolve experimentally. It should be noted that our conclusion contradicts that of Niemeyer, who assessed **1** to exist as a mixture of dimer and monomer in benzene based on cryoscopy measurements.[43] However, our DOSY measurements show no evidence of the monomeric species in solution.

To obtain the gold analogues of **1** and **2**, $(2,6\text{-}Mes_2C_6H_3)_2Fe$[30] was reacted with $Me_2S{\cdot}AuCl$. If the reaction was carried out and worked up at low temperature (<−30 °C), it is possible to obtain crystals of $(2,6\text{-}Mes_2C_6H_3)Au{\cdot}SMe_2$ (**5**; Scheme 2), the only example of a gold *m*-terphenyl complex that does not feature a phosphine ligand.[52,53] Complex **5** has been characterized by single-crystal X-ray diffraction (Figure S10), ^1H NMR spectroscopy, mass spectrometry, and elemental analysis. Compound **5** is unstable in solution at ambient temperatures and decomposes to a purple solid over 1−2 h, attributed to the formation of gold nanoparticles.[65] However, if $(2,6\text{-}Mes_2C_6H_3)_2Fe$[30] is allowed to react with $Me_2S{\cdot}AuCl$ at room temperature, extraction of the resultant purple solid into hexane and subsequent crystallization at −30 °C affords colorless crystals of **6**, the silver analogue of **1** and **2** (Scheme 2). The nature of this reaction means that **6** could only be obtained in very small quantities. Compound **6** is very thermally unstable with isolated crystals decomposing in a benzene-d_6 solution at room temperature within minutes. As a result, complex **6** has been characterized by single-crystal X-ray diffraction only (Figure 3 and Table 1), and no reaction yield has been determined. It should be noted that the diffraction data for **6** is low quality, featuring large residual electron density peaks that were modeled as free Au atoms with partial occupancy. This is attributed to a minor disorder or twin component that could not be satisfactorily modeled (see the CIF for further information). Nevertheless, the data are sufficient to confirm the connectivity of the molecule and give a reasonable estimate of the Au···Au distance [3.2312(6) Å],

Scheme 2. Reaction of $(2,6\text{-}Mes_2\text{-}C_6H_3)_2Fe$ with $Me_2S{\cdot}AuCl_2$ and Decomposition Pathways, Generating 5 and 6

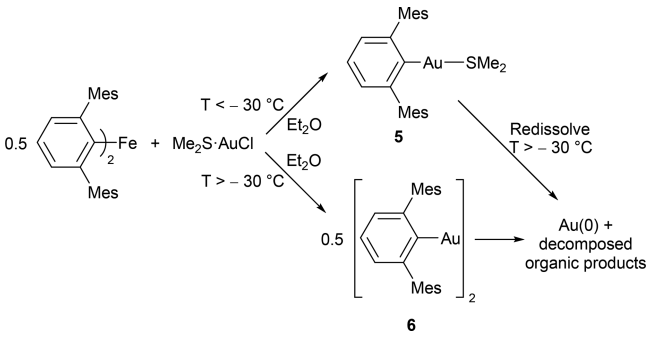

https://doi.org/10.1021/acs.inorgchem.0c03623
Inorg. Chem. 2021, 60, 10114−10123

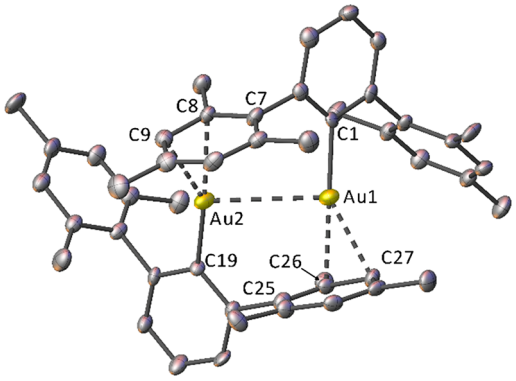

Figure 3. Crystal structure of **6** with displacement ellipsoids set to 50%. H atoms and disorder components omitted for clarity.

which is within the expected range for aurophilic interactions.[3,4]

Computational Analysis. Density functional theory (DFT) calculations were employed to probe the metal−metal interactions in **1**−**4** and **6** and to provide insight into the different geometries (terminal and bridged) that are observed in the solid-state structures. Geometry optimizations were performed on **1**−**4** and **6** using the PBEh-3c methodology[66] (as implemented in *ORCA 4.0.1*),[67,68] which is known to perform well for transition-metal complexes and for systems featuring noncovalent interactions.[66] In every case, the optimizations gave metal−metal distances, M−C (M = Cu, Ag, Au) σ-bond lengths, and bond angles about the metal centers in reasonable agreement with those found in the X-ray crystal structures (Tables S1 and S2).

To investigate the observed difference in the geometries between the Mes-substituted (**1** and **2**) and Xyl-substituted (**3** and **4**) complexes, geometry optimizations were carried out on models of these complexes in the alternative coordination mode (**1′**−**4′**; Figure S11). A comparison of the Gibbs free energies for the optimized structures (PBEh-3c) revealed that the terminal geometry is more stable in every case (by ca. 1.4−4.0 kcal mol^{-1}, Table S3). This suggests that, despite **3** and **4** adopting a bridged geometry in the solid state, there is no energetic preference for the bridged geometry in the gas phase. Thus, we propose that this geometry is observed because of the crystal packing effects rather than the bridged structures in **3** and **4** being inherently more stable. The small energy difference between the bridged and terminal geometries also correlates with the apparent fluxional nature of the complexes in solution, as evidenced by the NMR spectroscopic measurements (see above).

The bonding in **1**−**4** and **6** was analyzed using QTAIM, which rationalizes bonding by determining critical points (CPs) in the electron density function, $\rho(\mathbf{r})$,[54,55] and has previously been applied to group 11 metallophilic interactions.[69−76] QTAIM analysis was performed using *ORCA 4.0.1*[67,68] and the *MultiWFN 3.6* software package;[77] see section S3.1.2 for full details. Bond critical points (BCPs) were located between the metal centers for **1**, **2**, and **6**, suggesting a metallophilic interaction (Figure S13). Selected QTAIM parameters evaluated at the BCPs for these molecules are summarized in Table 2. The M1···M2 (M = Cu, Ag, Au) BCPs all display a relatively low electron density (ρ_{BCP}) and a small and positive Laplacian ($\nabla^2\rho_{BCP}$), which are typical of metal−metal interactions.[78,79]

Table 2. Selected Properties of the Electron Density at the BCPs According to QTAIM Analysis, as Well as Computed DIs (δ) between Appropriate Atom Pairs[a]

compound	interaction	$\rho(r)$	$\nabla^2\rho(r)$	DI (δ)	E_i (kcal mol^{-1})	BD	$\lvert V(r)\rvert/G(r)$
1	Cu1···Cu2	0.0339	0.0755	0.2885	−8.9	−0.138	1.20
	C1−Cu1	0.1172	0.2115	0.8142	−51.5	−0.474	1.51
	C19−Cu2	0.1175	0.2124	0.8154	−51.8	−0.476	1.51
	C7···Cu2	0.0585	0.1733	0.2744	−21.3	−0.208	1.22
	C25···Cu1	0.0578	0.1752	0.2674	−20.9	−0.197	1.21
2	Ag1···Ag2	0.0308	0.0810	0.3005	−8.1	−0.089	1.12
	C1−Ag1	0.1086	0.2217	0.8333	−43.1	−0.378	1.43
	C19−Ag2	0.1080	0.2212	0.8322	−42.8	−0.375	1.42
	C8···Ag2	0.0427	0.1279	0.2260	−12.5	−0.093	1.11
	C26···Ag1	0.0431	0.1290	0.2270	−12.7	−0.094	1.11
3	Cu1···Cu2			0.3291			
	C1−Cu1	0.1126	0.2204	0.7945	−49.5	−0.456	1.48
	C15−Cu1	0.0843	0.1790	0.5304	−32.7	−0.353	1.40
	C15−Cu2	0.0941	0.1898	0.6131	−37.8	−0.388	1.43
	C10···Cu2	0.0481	0.1514	0.2529	−16.4	−0.149	1.16
4	Ag1···Ag2			0.3365			
	C1−Ag1	0.1063	0.2269	0.8031	−42.3	−0.368	1.41
	C15−Ag1	0.0738	0.1668	0.5082	−24.4	−0.244	1.30
	C15−Ag2	0.0794	0.1798	0.5794	−27.0	−0.259	1.31
	C10···Ag2	0.0398	0.1199	0.2395	−11.3	−0.074	1.09
6	Au1···Au2	0.0199	0.0494	0.2379	−3.8	0.008	0.99
	C1−Au1	0.1465	0.1227	1.0252	−59.1	−0.538	1.72
	C19−Au2	0.1467	0.1230	1.0262	−59.2	−0.538	1.72
	C9···Au2	0.0556	0.1310	0.3181	−17.2	−0.200	1.25
	C27···Au1	0.0562	0.1303	0.3242	−17.5	−0.206	1.26

[a] $\rho(r)$ and $\nabla^2\rho(r)$ are given in standard atomic units.

https://doi.org/10.1021/acs.inorgchem.0c03623
Inorg. Chem. 2021, 60, 10114−10123

The $|V_{BCP}|/G_{BCP}$ ratio[78,80] (V_{BCP} = electronic potential energy at the BCP; G_{BCP} = electronic kinetic energy at the BCP) and the bond degree parameter (BD = H_{BCP}/ρ_{BCP}, where H_{BCP} = energy density at the BCP)[78,80] are two useful measures for characterizing heavier element−element bonds via QTAIM. The ratio $|V_{BCP}|/G_{BCP}$ distinguishes between pure closed-shell interactions (i.e., van der Waals or ionic bonds), where $|V_{BCP}|/G_{BCP} < 1$, and pure shared-shell interactions (i.e., fully covalent), where $|V_{BCP}|/G_{BCP} > 2$. Bonds that possess intermediate values ($1 < |V_{BCP}|/G_{BCP} < 2$) are classified as transit closed-shell interactions and feature some degree of covalency.[78,79] Metal−metal bonds typically fall in this transit closed-shell region,[78,79] and this is the case for **1** and **2**. For **6**, this value is <1, suggesting that the Au···Au interaction is purely closed-shell.

The BD gives a measure of the degree of covalency in these bonds, with more negative values indicating a greater covalent interaction.[78,80] The magnitude of this parameter decreases from **1** to **2**, consistent with a decrease in the covalency, and becomes positive for the closed-shell interaction in **6**. The interaction energy ($E_i = \frac{1}{2}V_{BCP}$)[81] provides an estimate of the strength of the metal−metal interaction for these compounds, which decreases in the order **1** > **2** ≫ **6**.

The delocalization indices (DIs, δ), a measure of the degree of electron sharing between atoms[82] that has been proposed as a quantum-mechanical measure of the bond order,[83] show a trend of **2** > **1** > **6** for the M···M interaction (Table 2), although the DIs of **1** and **2** are similar. The computed Mayer bond orders[84] (MBOs) for these metal−metal interactions follow a trend similar to that of the QTAIM parameters, with bond order reducing down the group (**1** = 0.35, **2** = 0.26, and **6** = 0.16). It should be noted that the computed QTAIM parameters for **1**, **2**, and **6** are broadly analogous to those found in previous studies on group 11 metallophilic interactions.[69−76]

In addition to the metal−metal interaction, QTAIM shows that each metal center in **1**, **2**, and **6** features one M−C σ bond (M1−C1 and M2−C19; M = Cu, Ag, Au) and one M···C_{arene} interaction. The C_{arene} bound to the metal center shifts across the series, moving from the *ipso*-C (**1**) to an *ortho*-C (**2**) and finally a *meta*-C (**6**). This can be attributed to the increasing M···M distance down the group. The computed QTAIM parameters for these interactions are given in Table 2 and demonstrate that the M−C σ bonds all show significant covalency (based on the BD and $|V_{BCP}|/G_{BCP}$ parameters) with large DIs consistent with a formal bond order of 1. The M···C_{arene} interactions also show significant covalency, although less so than the M−C σ bonds.

Compounds **3** and **4** do not feature a BCP between the metal centers (Figure S14). Instead, both metal centers bind to C15, with computed DIs of ca. 0.5 for M1−C15 and M2−C15 (M = Cu, Ag). In both compounds, the coordination sphere of M2 (M = Cu, Ag) is completed by coordination to C10, as evidenced by the presence of a BCP between M2 and C10. However, despite the lack of a BCP between the metal centers, the M1···M2 (M = Cu, Ag) DIs are larger than those observed in complexes **1** and **2** (Table 2). In addition, the MBOs for the metal−metal interactions in **3** and **4** (0.72 and 0.30, respectively) are larger than those for **1**, **2**, and **6** (see above).

The metal−metal interactions in **1**−**4** and **6** were analyzed further using an energy decomposition analysis employing natural orbitals for chemical valence (EDA-NOCV)[56−59] approach, as implemented in *ORCA 4.0.1*.[67,68] The total interaction energy (ΔE_{int}) between the two 2,6-$Ar_2C_6H_3M$ (Ar = Mes, Xyl; M = Cu, Ag, Au) fragments was decomposed into contributions from ΔE_{steric}, ΔE_{orb}, and ΔE_{disp} (Table 3). ΔE_{orb} and ΔE_{disp} are the orbital and dispersion contributions to ΔE_{int}, respectively. ΔE_{steric} is the combined electrostatic and Pauli-repulsion contribution.[85] The interaction energies for **1**−**4** and **6** are dominated by the ΔE_{orb} term, with positive values of ΔE_{steric} indicating that any electrostatic contributions to bonding are outweighed by the Pauli repulsion. Dispersion interactions are also found to contribute significantly, with ΔE_{disp} of ca. 20−25 kcal mol^{-1}. Despite its apparent instability in solution, compound **6** possesses ΔE_{int} (−65.15 kcal mol^{-1}) and ΔE_{orb} (−71.24 kcal mol^{-1}) comparable to those of **1** and **2**. We note that gold nanoparticles and Me_2S are generated in the synthesis of **6**, which could promote its degradation. In addition, reactions between **6** and the solvent (benzene or diethyl ether) could also contribute to its decomposition.

The ΔE_{orb} term can be further decomposed into complementary pairs of NOCVs, which represent the orbital interactions between the 2,6-$Ar_2C_6H_3M$ (Ar = Mes, Xyl; M = Cu, Ag, Au) fragments. For each pair of NOCVs, a deformation density plot ($\Delta\rho_k$), which represents the flow of charge between the molecular fragments, and its corresponding energy contribution to ΔE_{orb} (ΔE_k) can be calculated.[56−59] For **1**−**4** and **6**, $\Delta\rho$ values were calculated and visualized for all pairs of NOCVs that contributed at least 2 kcal mol^{-1} to ΔE_{orb}. For **1**, **2**, and **6**, most of these showed charge flow between the metal atoms and terphenyl ligands, with little charge flow to the region between the metal atoms (section S3.2.3 and Figures S15−S38). We interpret these to represent the metal−C_{arene} interactions. However, each complex had (at least) one $\Delta\rho$ plot that appeared to correspond to a metal−metal interaction. In these, electron density flows predominantly from the metal atoms to a region between them, with some contribution from the π system of the ligands (Figure 4). In **1**, $\Delta\rho_5$ and $\Delta\rho_8$ contribute a total of −8.537 kcal mol^{-1} to ΔE_{orb}, in **2**, $\Delta\rho_3$ contributes −5.161 kcal mol^{-1}, and in **6**, $\Delta\rho_6$ contributes −2.733 kcal mol^{-1}. This suggests that the strength of this metal−metal interaction decreases as the group is descended (Cu > Ag > Au). It also suggests that the main driving force for dimerization in **1**, **2**, and **6** is metal−C_{arene} interactions, although metallophilic interactions do make a small contribution.

For the bridged complexes (**3** and **4**), the $\Delta\rho$ plots suggest that ΔE_{orb} is dominated by M1···C15 and M2···C_{arene} interactions (M = Cu, Ag; section S3.2.3 and Figures S39−S51). In addition, many of the plots show electron density flowing from the metal centers to a region between them ($\Delta\rho_2$, $\Delta\rho_3$, $\Delta\rho_4$, and $\Delta\rho_6$ for **3**; $\Delta\rho_2$, $\Delta\rho_3$, and $\Delta\rho_6$ for **4**; Figures S39−S51), suggesting a metal−metal bonding interaction.

Table 3. Energy Decomposition Analysis for Compounds 1−4 and 6[a]

compound	ΔE_{int}	ΔE_{steric}	ΔE_{orb}	ΔE_{disp}
1	−82.40	+16.05	−74.03	−24.42
2	−63.96	+9.23	−51.65	−21.54
3	−88.45	+4.31	−70.16	−22.60
4	−76.08	+5.56	−60.06	−21.58
6	−65.15	+25.81	−71.24	−19.73

[a]All values in kcal mol^{-1}. $\Delta E_{int} = \Delta E_{steric} + \Delta E_{orb} + \Delta E_{disp}$.

https://doi.org/10.1021/acs.inorgchem.0c03623
Inorg. Chem. 2021, 60, 10114−10123

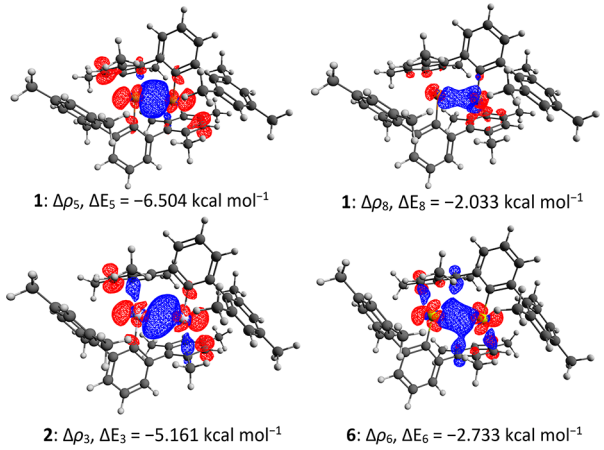

Figure 4. Selected deformation densities associated with metal−metal interactions in **1**, **2**, and **6**. The charge flow is from the negative isosurface (red) to the positive isosurface (blue). All isosurfaces are plotted at 0.0005 au. Visualizations are rendered in *Avogadro v1.2.0*.[86]

However, unlike compounds **1**, **2**, and **6**, none of these $\Delta\rho$ plots are dominated by the metal−metal interaction; all feature significant contributions from M1···C15 and M2···C_{arene} interactions. As such, it is difficult to quantitatively estimate the contribution to ΔE_{orb} of the metal−metal interactions in **3** and **4**.

The EDA-NOCV analysis thus suggests that there is a metallophilic bonding interaction in **3** and **4** despite the lack of a BCP in the QTAIM analysis. A similar phenomenon was observed in platinum(II)/gold(I)[87] and palladium(II)/copper(I)[88,89] bimetallic complexes featuring metal atoms bridged by a single C atom. In both cases, EDA-NOCV analyses suggest that a metallophilic interaction is present despite no BCP being identified in a QTAIM analysis.[87−89] In related QTAIM analyses, a palladium(II)/zinc(II) bimetallic complex featuring a bridging C atom was found to possess a Pd−Zn bond path but no Zn−C bond path.[89,90] These studies, together with our analyses for **3** and **4**, suggest that employing complementary QTAIM *and* EDA-NOCV analyses is advantageous for the study of metallophilic interactions, particularly in complexes featuring bridging C atoms.

Our QTAIM and EDA-NOCV analyses suggest that, for **1**, **2**, and **6**, the strength of the metallophilic interaction decreases as the group is descended (Cu > Ag > Au). This is noteworthy because early theoretical work employing Hartree−Fock (HF) and perturbation (MP2) theories suggested that aurophilic interactions in the $[X{-}Au{-}PH_3]_2$ model system (X = F, Cl, Br, I, CH_3, SCH_3) arise from dispersion forces that are strengthened through relativistic effects.[91,92] Subsequent MP2 calculations on $[X{-}M{-}PH_3]_2$ (X = H, Cl; M = Cu, Ag, Au) concluded that metallophilic interactions increase in strength as group 11 is descended (Au > Ag > Cu) because of relativistic effects.[93] However, later work employing quadratic configuration interaction with singles and doubles (QCISD) and coupled-cluster methods on $[Cl{-}M{-}PH_3]_2$ (M = Cu, Ag, Au) suggested that aurophilic interactions are weaker than argentophilic (by ca. 1 kcal mol^{-1}).[94] The debate over the origin and strength of metallophilic interactions remains vigorous, with orbital interactions, dispersion interactions, electrostatics, relativistic effects, and Pauli repulsion all hypothesized to play a role.[22−27] While consensus has not been reached, recent studies suggest that metallophilic interactions are relatively weak with other factors, including dispersion forces between the ligands, supporting dimerization.[22,26,27] This aligns with our EDA-NOCV analyses, which suggest that metallophilic interactions in **1**, **2**, and **6** make small contributions to ΔE_{orb} (Table 3 and Figure 4). In a recent study, high-level coupled-cluster singles and doubles with perturbative triples calculations were carried out on crystallographically characterized gold(I) and silver(I) complexes which feature longer Au···Au distances relative to the Ag···Ag distances. The longer Au···Au distances are attributed to relativistic effects enhancing Pauli repulsion in the Au···Au interactions relative to the Ag···Ag interactions.[24] This observation aligns with the EDA-NOCV analyses for **1**, **2**, and **6**, in which **6** possesses a larger ΔE_{steric} term than **1** or **2** (by ca. 10−15 kcal mol^{-1}; Table 3). Higher-level coupled-cluster calculations could provide further insight into these metallophilic interactions, and this will be investigated in future work.

■ CONCLUSIONS

Metathesis reactions of $(2,6\text{-}Mes_2C_6H_3)_2Fe$ or $(2,6\text{-}Xyl_2C_6H_3)_2Fe$ with group 11 M(I) triflate salts (M = Cu, Ag) afforded the dimeric complexes **1**−**4**, which were characterized by a variety of spectroscopic techniques. Single-crystal X-ray diffraction reveals the complexes to adopt different geometries (terminal or bridged) depending on the identity of the *m*-terphenyl ligand. NMR spectroscopy measurements, including DOSY, suggest that **1**−**4** remain dimeric but fluxional in a benzene-d_6 solution. The reaction between $(2,6\text{-}Mes_2C_6H_3)_2Fe$ and $Me_2S{\cdot}AuCl$ at $T < -30$ °C allowed for isolation and characterization of the gold(I) *m*-terphenyl complex **5**. This complex decomposes in solution at $T > -30$ °C; however, it was possible to isolate a few crystals of **6** [the gold(I) analogue of **1** and **2**] from this mixture that were suitable for single-crystal X-ray diffraction. DFT calculations suggest that there is a small energetic preference (ca. 1.4−4.0 kcal mol^{-1}) for the terminal relative to the bridged structures for **1**−**4** in the gas phase, and we attribute the bridged structure observed in the solid state for **3** and **4** to crystal packing effects. The existence of metallophilic interactions in complexes **1**, **2**, and **6** (terminal geometry) is supported by QTAIM analysis on DFT-optimized structures. By contrast, the same analysis of **3** and **4** (bridged geometry) reveals no BCP between the metal centers. However, EDA-NOCV analysis of **1**−**4** and **6** suggests that a metallophilic interaction *is* present in **3** and **4**, although the strength of this interaction is difficult to quantify. For **1**, **2**, and **6**, EDA-NOCV analysis reveals small contributions to ΔE_{orb} (ca. 2.5−8.5 kcal mol^{-1}), which can be assigned predominantly to a metallophilic interaction. Both QTAIM and EDA-NOCV analyses suggest that the strength of the metallophilic interaction in **1**, **2**, and **6** decreases as the group is descended (Cu > Ag > Au).

■ EXPERIMENTAL SECTION

General Experimental Procedures. All experiments were carried out under an inert atmosphere (argon or nitrogen) using standard Schlenk line (argon) and glovebox (nitrogen) techniques. Diethyl ether, THF, toluene, and isohexane were dried by passing through a column of activated 4 Å molecular sieves (SPS). Solvents were stored over 3 Å molecular sieves (THF) or a potassium mirror (diethyl ether, toluene, and isohexane) and degassed in vacuo prior to use. C_6D_6 was dried over molten potassium and purified by vacuum transfer before being degassed (three freeze−pump−thaw cycles) and

https://doi.org/10.1021/acs.inorgchem.0c03623
Inorg. Chem. 2021, 60, 10114−10123

stored over a potassium mirror prior to use. ^{1}H and ^{13}C{^{1}H} NMR spectra were recorded on Bruker AV(III)400HD and AV(III)500HD spectrometers with chemical shifts reported relative to tetramethylsilane. DOSY NMR (convection compensated) experiments were carried out using the pulsed-field gradient spin−echo NMR diffusion methods and analyzed with the software implemented by Bruker on an AV(III)400HD NMR spectrometer. Diffusion constants (D) were obtained directly from the software, and hydrodynamic radii (r_H) were calculated from the Stokes−Einstein equation: $r_H = kT/6\pi\eta D$ (where T is the absolute temperature, k is the Boltzmann constant, η is the solvent viscosity, and D is the coefficient of diffusion). Averaged molecular radii were estimated from the calculated molecular volume defined as the volume inside a contour of 0.001 electrons/bohr.[3] High-resolution mass spectrometry was performed on a Bruker Impact II spectrometer with an APCI II source and a direct probe attachment. Elemental analysis was performed on an Exeter Analytical, Inc., CE-440 elemental analyzer, with samples combusted at temperatures of 975 °C before being measured. The complexes (2,6-$Mes_2C_6H_3$)$_2$Fe, (2,6-$Xyl_2C_6H_3$)$_2$Fe, and Me_2S·AuCl were synthesized according to the literature.[30,60,95] A copper(I) triflate/benzene complex and silver(I) triflate were purchased commercially and used without further purification. Note that all reactions involving silver(I) triflate were carried out under low light and the resulting products stored in the dark. Details of the crystallographic and computational methods can be found in sections S2.1 and S3.1, respectively.

Synthesis and Characterization. *[2,6-$Mes_2C_6H_3Cu]_2$ (**1**).* To a mixture of (2,6-$Mes_2C_6H_3$)$_2$Fe (150 mg, 0.22 mmol) and [CF_3SO_3Cu]$_2$·C_6H_6 (111 mg, 0.22 mmol) was added diethyl ether (30 mL), resulting in a white suspension, which was stirred at room temperature for 16 h. Removal of solvent in vacuo afforded a white solid, which was extracted into isohexane (3 × 15 mL), filtering to remove all insoluble material. The filtrate was concentrated to ca. 20 mL and kept at −30 °C for 48 h to obtain green-yellow crystals of **1** suitable for X-ray diffraction. Yield: 112 mg (68%). ^{1}H NMR (400 MHz, C_6D_6, 298 K): δ 2.02 (12H, s, *o*-Me of Mes), 2.20 (6H, s, *p*-Me of Mes), 6.71 (4H, s, *m*-H of Mes), 6.81 (2H, d, J = 7.4 Hz, *m*-H of C_6H_3), 7.13 (1H, t, J = 7.4 Hz, *p*-H of C_6H_3). ^{13}C{^{1}H} NMR (101 MHz, C_6D_6, 298 K): δ 21.2 (*p*-Me of Mes), 21.9 (*o*-Me of Mes), 124.6 (*m*-CH of C_6H_3), 126.7 (*p*-CH of C_6H_3), 127.3 (*m*-CH of Mes), 133.8 (*o*-C of Mes), 134.2 (*p*-C of Mes), 143.5 (*i*-C of Mes), 152.4 (*o*-C of C_6H_3), 159.7 (*i*-C of C_6H_3). Molecular radius (Å) [average diffusion coefficient (m^2 s^{-1}) measured by DOSY NMR in C_6D_6: 7.06 × 10^{-10}]. Calcd for dimer: 5.24. Found: 5.13. HRMS (APCI). Calcd for [$C_{48}H_{50}Cu_2$]$^+$: m/z 752.2499. Found: m/z 752.2495. Elem anal. Calcd for $C_{48}H_{50}Cu_2$: C, 76.46; H: 6.68. Found: C, 76.73; H, 6.68.

*[2,6-$Mes_2C_6H_3Ag]_2$ (**2**).* To a mixture of (2,6-$Mes_2C_6H_3$)$_2$Fe (100 mg, 0.15 mmol) and CF_3SO_3Ag (75 mg, 0.29 mmol) was added diethyl ether (30 mL), resulting in a white suspension, which was stirred at room temperature for 16 h. Removal of solvent in vacuo afforded a white solid, which was extracted into isohexane (3 × 15 mL), filtering to remove all insoluble material. The filtrate was concentrated to ca. 20 mL and kept at −30 °C for 48 h to obtain colorless crystals of **2** suitable for X-ray diffraction. Yield: 106 mg (86%). ^{1}H NMR (500 MHz, C_6D_6, 298 K): δ 2.04 (12H, s, *o*-Me of Mes), 2.17 (6H, s, *p*-Me of Mes), 6.75 (4H, s, *m*-H of Mes), 6.96 (2H, d, J = 7.5 Hz, *m*-H of C_6H_3), 7.18 (1H, t, J = 7.5 Hz, *p*-H of C_6H_3). ^{13}C{^{1}H} NMR (126 MHz, C_6D_6, 298 K): δ 21.1 (*p*-Me of Mes), 22.2 (*o*-Me of Mes), 124.3 (*m*-CH of C_6H_3), 126.5 (*p*-CH of C_6H_3), 127.6 (*m*-CH of Mes), 134.2 (*o*-C of Mes), 136.5 (*p*-C of Mes), 147.9 (*i*-C of Mes), 154.4 (*o*-C of C_6H_3), 161.6 (*i*-C of C_6H_3). Molecular radius (Å) [average diffusion coefficient (m^2 s^{-1}) measured by DOSY NMR in C_6D_6: 7.29 × 10^{-10}]. Calcd for dimer: 5.27. Found: 4.97. HRMS (APCI). Calcd for [$C_{48}H_{50}Ag_2$]$^+$: m/z 840.2009. Found: m/z 840.2034. Elem anal. Calcd for $C_{48}H_{50}Ag_2$: C, 68.42; H, 5.98. Found: C, 68.30; H, 5.82.

*[2,6-$Xyl_2C_6H_3Cu]_2$ (**3**).* To a mixture of (2,6-$Xyl_2C_6H_3$)$_2$Fe (200 mg, 0.32 mmol) and [CF_3SO_3Cu]$_2$·C_6H_6 (161 mg, 0.32 mmol) was added diethyl ether (30 mL), resulting in a white suspension, which was stirred at room temperature for 16 h. The solvent was removed in vacuo and extracted by toluene (3 × 10 mL), filtering to remove all insoluble material. The toluene was then removed in vacuo and the resulting solid extracted by diethyl ether (3 × 20 mL), filtering to remove all insoluble material. The filtrate was then concentrated to ca. 20 mL and kept at −30 °C for 48 h to obtain colorless crystals of **3** suitable for X-ray diffraction. Yield: 97 mg (44%). ^{1}H NMR (400 MHz, C_6D_6, 298 K): δ 2.00 (12H, s, *o*-Me of Xyl), 6.74 (2H, d, J = 7.4 Hz, *m*-H of C_6H_3), 6.82 (4H, d, J = 7.4 Hz, *m*-H of Xyl), 6.91 (2H, t, J = 7.4 Hz, *p*-H of Xyl), 7.10 (1H, t, J = 7.4 Hz, *p*-H of C_6H_3). ^{13}C{^{1}H} NMR (101 MHz, C_6D_6, 298 K): δ 21.9 (*o*-Me of Xyl), 124.4 (*m*-CH of C_6H_3), 125.3 (*p*-CH of Xyl), 126.4 (*m*-CH of Xyl), 126.8 (*p*-CH of C_6H_3), 134.5 (*o*-C of Xyl), 146.3 (*i*-C of Xyl), 152.5 (*o*-C of C_6H_3), 158.5 (*i*-C of C_6H_3). Molecular radius (Å) [average diffusion coefficient (m^2 s^{-1}) measured by DOSY NMR in C_6D_6: 7.38 × 10^{-10}]. Calcd for dimer: 4.97. Found: 4.91. HRMS (APCI). Calcd for [$C_{44}H_{42}Cu_2$]$^+$: m/z 696.1873. Found: m/z 696.1872. Elem anal. Calcd for $C_{44}H_{42}Cu_2$: C, 75.72; H, 6.07. Found: C, 75.83; H, 5.95.

*[2,6-$Xyl_2C_6H_3Ag]_2$ (**4**).* To a mixture of (2,6-$Xyl_2C_6H_3$)$_2$Fe (150 mg, 0.24 mmol) and CF_3SO_3Ag (123 mg, 0.48 mmol) was added diethyl ether (30 mL), resulting in a white suspension, which was stirred at room temperature for 16 h. The solvent was removed in vacuo and extracted by toluene (3 × 10 mL), filtering to remove all insoluble material. The toluene was then removed in vacuo and the resulting solid extracted by diethyl ether (3 × 20 mL), filtering to remove all insoluble material. The filtrate was then concentrated to ca. 20 mL and kept at −30 °C for 48 h to obtain colorless crystals of **4** suitable for X-ray diffraction. Yield: 163 mg (87%). ^{1}H NMR (500 MHz, C_6D_6, 298 K): δ 2.01 (12H, s, *o*-Me of Xyl), 6.88 (6H, br s, *m*- and *p*-H of Xyl), 6.90 (2H, d, J = 7.5 Hz, *m*-H of C_6H_3), 7.16 (1H, t, J = 7.5 Hz, *p*-H of C_6H_3). ^{13}C{^{1}H} NMR (126 MHz, C_6D_6, 298 K): δ 22.3 (*o*-Me of Xyl), 123.6 (*m*-CH of C_6H_3), 124.1 (*p*-CH of Xyl), 125.9 (*m*-CH of Xyl), 128.4 (*p*-CH of C_6H_3), 137.0 (*o*-C of Xyl), 150.7 (*i*-C of Xyl), 154.9 (*o*-C of C_6H_3), 159.2 (*i*-C of C_6H_3). Molecular radius (Å) [average diffusion coefficient (m^2 s^{-1}) measured by DOSY NMR in C_6D_6: 7.24 × 10^{-10}]. Calcd for dimer: 5.00. Found: 4.88. HRMS (APCI). Calcd for [$C_{44}H_{42}Ag_2$]$^+$: m/z 784.1383. Found: m/z 784.1370. Elem anal. Calcd for $C_{44}H_{42}Ag_2$: C, 67.19; H, 5.38. Found: C, 67.34; H, 5.36.

*(2,6-$Mes_2C_6H_3$)Au·SMe_2 (**5**).* To a mixture of (2,6-$Mes_2C_6H_3$)$_2$Fe (100 mg, 0.15 mmol) and Me_2S·AuCl (82 mg, 0.28 mmol) was added diethyl ether (30 mL) at −78 °C with stirring, resulting in a white suspension, which was maintained at −78 °C for 4 h. The reaction mixture was filtered and concentrated (maintaining temperatures of <−30 °C) to obtain colorless crystals of **5** suitable for X-ray diffraction. Yield: 78.8 mg (47%). ^{1}H NMR (400 MHz, C_6D_6, 298 K): δ 1.22 (6H, s, Me of SMe_2), 2.26 (6H, s, *p*-Me of Mes), 2.35 (12H, s, *o*-Me of Mes), 6.92 (4H, s, *m*-H of Mes), 7.17 (2H, d, J = 7.4 Hz, *m*-H of C_6H_3), 7.30 (1H, t, J = 7.4 Hz, *p*-H of C_6H_3). HRMS (APCI). Calcd for [$C_{26}H_{31}AuS$]$^+$: m/z 572.1807. Found: m/z 572.1789. Elem anal. Calcd for $C_{26}H_{31}AuS$: C, 54.54; H, 5.46. Found: C, 54.85; H, 5.46.

*[2,6-$Mes_2C_6H_3Au]_2$ (**6**).* To a mixture of (2,6-$Mes_2C_6H_3$)$_2$Fe (100 mg, 0.15 mmol) and Me_2S·AuCl (86 mg, 0.29 mmol) was added diethyl ether (30 mL), resulting in a white suspension, which was stirred at room temperature for 16 h. Purple residues were obtained after removal of the solvent in vacuo and extracted by isohexane (3 × 15 mL), filtering to obtain a colorless solution, which was concentrated to ca. 10 mL and kept at −30 °C for 48 h to obtain colorless crystals of **3** suitable for X-ray diffraction.

■ ASSOCIATED CONTENT

Supporting Information

The Supporting Information is available free of charge at https://pubs.acs.org/doi/10.1021/acs.inorgchem.0c03623.

^{1}H and ^{13}C{^{1}H} NMR spectra, crystallographic data, and details of computational calculations (PDF)

Imaginary vibration of methyl group torsion in **2** (XYZ)

https://doi.org/10.1021/acs.inorgchem.0c03623
Inorg. Chem. 2021, 60, 10114−10123

Imaginary vibration of methyl group torsion in **2′** (XYZ)
Imaginary vibration of a rocking of the xylyl group coordinated to Cu2 in **3** (XYZ)

Accession Codes

CCDC 2047551−2047556 contain the supplementary crystallographic data for this paper. These data can be obtained free of charge via www.ccdc.cam.ac.uk/data_request/cif, or by emailing data_request@ccdc.cam.ac.uk, or by contacting The Cambridge Crystallographic Data Centre, 12 Union Road, Cambridge CB2 1EZ, UK; fax: +44 1223 336033.

AUTHOR INFORMATION

Corresponding Author

Deborah L. Kays − *School of Chemistry, University Park, University of Nottingham, Nottingham NG7 2RD, U.K.*; orcid.org/0000-0002-4616-6001; Email: deborah.kays@nottingham.ac.uk

Authors

Yu Liu − *School of Chemistry, University Park, University of Nottingham, Nottingham NG7 2RD, U.K.*

Laurence J. Taylor − *School of Chemistry, University Park, University of Nottingham, Nottingham NG7 2RD, U.K.*; orcid.org/0000-0002-4948-4267

Stephen P. Argent − *School of Chemistry, University Park, University of Nottingham, Nottingham NG7 2RD, U.K.*

Jonathan McMaster − *School of Chemistry, University Park, University of Nottingham, Nottingham NG7 2RD, U.K.*; orcid.org/0000-0003-0917-7454

Complete contact information is available at: https://pubs.acs.org/10.1021/acs.inorgchem.0c03623

Notes

The authors declare no competing financial interest.

ACKNOWLEDGMENTS

We acknowledge the EPSRC (Grant EP/R004064/1) and the University of Nottingham (Vice-Chancellor's Scholarship for Research Excellence to Y.L.) for financial support of this research. We are grateful for access to the University of Nottingham's Augusta High Performance Computer. We also thank Ben Pointer-Gleadhill and Dr. Tong Liu of the University of Nottingham Analytical Services Department for mass spectrometry and elemental microanalysis measurements, respectively.

REFERENCES

(1) Pyykkö, P. Strong Closed-Shell Interactions in Inorganic Chemistry. *Chem. Rev.* **1997**, *97* (3), 597−636.

(2) Sculfort, S.; Braunstein, P. Intramolecular d^{10}-d^{10} Interactions in Heterometallic Clusters of the Transition Metals. *Chem. Soc. Rev.* **2011**, *40* (5), 2741−2760.

(3) Schmidbaur, H.; Schier, A. A Briefing on Aurophilicity. *Chem. Soc. Rev.* **2008**, *37* (9), 1931−1951.

(4) Schmidbaur, H.; Schier, A. Aurophilic Interactions as a Subject of Current Research: An up-Date. *Chem. Soc. Rev.* **2012**, *41* (1), 370−412.

(5) Schmidbaur, H.; Schier, A. Argentophilic Interactions. *Angew. Chem., Int. Ed.* **2015**, *54* (3), 746−784.

(6) Harisomayajula, N. V. S.; Makovetskyi, S.; Tsai, Y. C. Cuprophilic Interactions in and between Molecular Entities. *Chem. - Eur. J.* **2019**, *25* (38), 8936−8954.

(7) Katz, M. J.; Sakai, K.; Leznoff, D. B. The Use of Aurophilic and Other Metal-Metal Interactions as Crystal Engineering Design Elements to Increase Structural Dimensionality. *Chem. Soc. Rev.* **2008**, *37* (9), 1884−1895.

(8) Wong, K. M.-C.; Yam, V. W.-W. Self-Assembly of Luminescent Alkynylplatinum(II) Terpyridyl Complexes: Modulation of Photophysical Properties through Aggregation Behavior. *Acc. Chem. Res.* **2011**, *44* (6), 424−434.

(9) Po, C.; Tam, A. Y.-Y.; Wong, K. M.-C.; Yam, V. W.-W. Supramolecular Self-Assembly of Amphiphilic Anionic Platinum(II) Complexes: A Correlation between Spectroscopic and Morphological Properties. *J. Am. Chem. Soc.* **2011**, *133* (31), 12136−12143.

(10) Au-Yeung, H.-L.; Leung, S. Y.-L.; Tam, A. Y.-Y.; Yam, V. W.-W. Transformable Nanostructures of Platinum-Containing Organosilane Hybrids: Non-Covalent Self-Assembly of Polyhedral Oligomeric Silsesquioxanes Assisted by Pt···Pt and π-π Stacking Interactions of Alkynylplatinum(II) Terpyridine Moieties. *J. Am. Chem. Soc.* **2014**, *136* (52), 17910−17913.

(11) Xie, J.; Zheng, Y.; Ying, J. Y. Highly Selective and Ultrasensitive Detection of Hg^{2+} Based on Fluorescence Quenching of Au Nanoclusters by Hg^{2+}-Au^{+} Interactions. *Chem. Commun.* **2010**, *46* (6), 961−963.

(12) Yam, V. W.-W.; Cheng, E. C.-C. Highlights on the Recent Advances in Gold Chemistry—a Photophysical Perspective. *Chem. Soc. Rev.* **2008**, *37* (9), 1806−1813.

(13) Yam, V. W.-W.; Au, V. K.-M.; Leung, S. Y.-L. Light-Emitting Self-Assembled Materials Based on d^8 and d^{10} Transition Metal Complexes. *Chem. Rev.* **2015**, *115* (15), 7589−7728.

(14) Ni, W.-X.; Li, M.; Zheng, J.; Zhan, S.-Z.; Qiu, Y.-M.; Ng, S. W.; Li, D. Approaching White-Light Emission from a Phosphorescent Trinuclear Gold(I) Cluster by Modulating Its Aggregation Behavior. *Angew. Chem., Int. Ed.* **2013**, *52* (50), 13472−13476.

(15) Weber, D.; Tarselli, M. A.; Gagné, M. R. Mechanistic Surprises in the Gold(I)-Catalyzed Intramolecular Hydroarylation of Allenes. *Angew. Chem., Int. Ed.* **2009**, *48* (31), 5733−5736.

(16) Heckler, J. E.; Zeller, M.; Hunter, A. D.; Gray, T. G. Geminally Diaurated Gold(I) Aryls from Boronic Acids. *Angew. Chem., Int. Ed.* **2012**, *51* (24), 5924−5928.

(17) Weber, D.; Jones, T. D.; Adduci, L. L.; Gagné, M. R. Strong Electronic and Counterion Effects on Geminal Digold Formation and Reactivity as Revealed by Gold(I)-Aryl Model Complexes. *Angew. Chem., Int. Ed.* **2012**, *51* (10), 2452−2456.

(18) Gómez-Suárez, A.; Nolan, S. P. Dinuclear Gold Catalysis: Are Two Gold Centers Better than One? *Angew. Chem., Int. Ed.* **2012**, *51* (33), 8156−8159.

(19) Brown, T. J.; Weber, D.; Gagné, M. R.; Widenhoefer, R. A. Mechanistic Analysis of Gold(I)-Catalyzed Intramolecular Allene Hydroalkoxylation Reveals an off-Cycle Bis(Gold) Vinyl Species and Reversible C-O Bond Formation. *J. Am. Chem. Soc.* **2012**, *134* (22), 9134−9137.

(20) Smirnova, E. S.; Echavarren, A. M. A Hexanuclear Gold Cluster Supported by Three-Center-Two-Electron Bonds and Aurophilic Interactions. *Angew. Chem., Int. Ed.* **2013**, *52* (34), 9023−9026.

(21) Zhdanko, A.; Maier, M. E. The Mechanism of Gold(I)-Catalyzed Hydroalkoxylation of Alkynes: An Extensive Experimental Study. *Chem. - Eur. J.* **2014**, *20* (7), 1918−1930.

(22) Zheng, Q.; Borsley, S.; Nichol, G. S.; Duarte, F.; Cockroft, S. L. The Energetic Significance of Metallophilic Interactions. *Angew. Chem., Int. Ed.* **2019**, *58* (36), 12617−12623.

(23) Brands, M. B.; Nitsch, J.; Guerra, C. F. Relevance of Orbital Interactions and Pauli Repulsion in the Metal-Metal Bond of Coinage Metals. *Inorg. Chem.* **2018**, *57* (5), 2603−2608.

(24) Wan, Q.; Yang, J.; To, W. P.; Che, C. M. Strong Metal-Metal Pauli Repulsion Leads to Repulsive Metallophilicity in Closed-Shell d^8 and d^{10} Organometallic Complexes. *Proc. Natl. Acad. Sci. U. S. A.* **2021**, *118* (1), No. e2019265118.

(25) Wuttke, A.; Feldt, M.; Mata, R. A. All That Binds Is Not Gold—The Relative Weight of Aurophilic Interactions in Complex Formation. *J. Phys. Chem. A* **2018**, *122*, 6918−6925.

(26) Grimme, S.; Djukic, J. P. Cation-Cation "Attraction": When London Dispersion Attraction Wins over Coulomb Repulsion. *Inorg. Chem.* **2011**, *50* (6), 2619−2628.
(27) Andrejić, M.; Mata, R. A. Study of Ligand Effects in Aurophilic Interactions Using Local Correlation Methods. *Phys. Chem. Chem. Phys.* **2013**, *15* (41), 18115−18122.
(28) Twamley, B.; Haubrich, S. T.; Power, P. P. Element Derivatives of Sterically Encumbering Terphenyl Ligands. In *Advances in Organometallic Chemistry*; West, R., Hill, A. F., Eds.; Academic Press, 1999; Vol. *44*, pp 1−65.
(29) Clyburne, J. A. C.; McMullen, N. Unusual Structures of Main Group Organometallic Compounds Containing *m*-Terphenyl Ligands. *Coord. Chem. Rev.* **2000**, *210* (1), 73−99.
(30) Kays, D. L.; Cowley, A. R. Monomeric, Two-Coordinate Mn, Fe and Co(II) Complexes Featuring 2,6-(2,4,6-Trimethylphenyl)-Phenyl Ligands. *Chem. Commun.* **2007**, 1053−1055.
(31) Kays, D. L. The Stabilisation of Organometallic Complexes Using *m*-Terphenyl Ligands. *In Organometallic Chemistry* **2010**, *36*, 56−76.
(32) Rivard, E.; Power, P. P. Multiple Bonding in Heavier Element Compounds Stabilized by Bulky Terphenyl Ligands. *Inorg. Chem.* **2007**, *46* (24), 10047−10064.
(33) Carrasco, M.; Mendoza, I.; Faust, M.; López-Serrano, J.; Peloso, R.; Rodríguez, A.; Álvarez, E.; Maya, C.; Power, P. P.; Carmona, E. Terphenyl Complexes of Molybdenum and Tungsten with Quadruple Metal-Metal Bonds and Bridging Carboxylate Ligands. *J. Am. Chem. Soc.* **2014**, *136* (25), 9173−9180.
(34) Carrasco, M.; Mendoza, I.; Álvarez, E.; Grirrane, A.; Maya, C.; Peloso, R.; Rodríguez, A.; Falceto, A.; Álvarez, S.; Carmona, E. Experimental and Computational Studies of the Molybdenum-Flanking Arene Interaction in Quadruply Bonded Dimolybdenum Complexes with Terphenyl Ligands. *Chem. - Eur. J.* **2015**, *21* (1), 410−421.
(35) Ni, C.; Power, P. P. Transition Metal Complexes Stabilized by Bulky Terphenyl Ligands: Application to Metal-Metal Bonded Compounds. In *Structure and Bonding*; Parkin, G., Ed.; Springer: Berlin, 2010; Vol. *136*, pp 59−112.
(36) Nguyen, T.; Sutton, A. D.; Brynda, M.; Fettinger, J. C.; Long, G. J.; Power, P. P. Synthesis of a Stable Compound with Fivefold Bonding between Two Chromium(I) Centers. *Science* **2005**, *310*, 844−847.
(37) Wolf, R.; Ni, C.; Nguyen, T.; Brynda, M.; Long, G. J.; Sutton, A. D.; Fischer, R. C.; Fettinger, J. C.; Hellman, M.; Pu, L.; Power, P. P. Substituent Effects in Formally Quintuple-Bonded ArCrCrAr Compounds (Ar = Terphenyl) and Related Species. *Inorg. Chem.* **2007**, *46* (26), 11277−11290.
(38) He, X.; Olmstead, M. M.; Power, P. P. Synthesis of $[Me_2SCu(C_6H_2\text{-}2,4,6\text{-}t\text{-}Bu_3)]$ and $[(Me_2S)_2Cu(\mu\text{-}C_6H_2\text{-}2,4,6\text{-}Ph_3)\text{-}Cu(C_6H_2\text{-}2,4,6\text{-}Ph_3)]$: Mononuclear and Dinuclear Organocopper(I) Species of Formula $[CuR{\cdot}Solvate]_{1\ or\ 2}$. *J. Am. Chem. Soc.* **1992**, *114* (24), 9668−9670.
(39) Hwang, C.-S.; Power, P. P. Isolation and Structural Characterization of the Lithium Cyanoorganocuprate Salt $[Li(THF)_2\{Cu(CN)C_6H_3\text{-}2,6\text{-}Trip_2\}]_2$ (Trip = $-C_6H_2\text{-}2,4,6\text{-}i\text{-}Pr_3$). *J. Am. Chem. Soc.* **1998**, *120* (25), 6409−6410.
(40) Groysman, S.; Holm, R. H. A Series of Mononuclear Quasi-Two-Coordinate Copper(I) Complexes Employing a Sterically Demanding Thiolate Ligand. *Inorg. Chem.* **2009**, *48* (2), 621−627.
(41) Groysman, S.; Majumdar, A.; Zheng, S. L.; Holm, R. H. Reactions of Monodithiolene Tungsten(VI) Sulfido Complexes with Copper(I) in Relation to the Structure of the Active Site of Carbon Monoxide Dehydrogenase. *Inorg. Chem.* **2010**, *49* (3), 1082−1089.
(42) Rungthanaphatsophon, P.; Barnes, C. L.; Walensky, J. R. Copper(I) Clusters with Bulky Dithiocarboxylate, Thiolate, and Selenolate Ligands. *Dalton Trans.* **2016**, *45* (36), 14265−14276.
(43) Niemeyer, M. σ-Carbon versus π-Arene Interactions in the Solid-State Structures of Trimeric and Dimeric Copper Aryls $(CuAr)_n$ (n = 3, Ar = $2,6\text{-}Ph_2C_6H_3$; n = 2, Ar = $2,6\text{-}Mes_2C_6H_3$). *Organometallics* **1998**, *17* (21), 4649−4656.
(44) Klett, J.; Klinkhammer, K. W.; Niemeyer, M. Ligand Exchange between Arylcopper Compounds and Bis(hypersilyl)tin or Bis-(hypersilyl)lead: Synthesis and Characterization of Hypersilylcopper and a Stannanediyl Complex with a Cu-Sn Bond. *Chem. - Eur. J.* **1999**, *5* (9), 2531−2536.
(45) Lang, H.; Köhler, K.; Rheinwald, G.; Zsolnai, L.; Büchner, M.; Driess, A.; Huttner, G.; Strähle, J. Monomeric Alkyne-Stabilized Complexes of Organo-Copper(I) and -Silver(I). *Organometallics* **1999**, *18* (4), 598−605.
(46) Hwang, C.-S.; Power, P. P. Synthesis and Characterization of the Organoiodocuprate Complexes $[Li(THF)_4][2,6\text{-}Mes_2H_3C_6Cu_2I_2]$ (Mes = $C_6H_2\text{-}2,4,6\text{-}Me_3$) and $(Et_2O)_2Li\{ICuC_6H_3\text{-}2,6\text{-}Trip_2\}$ (Trip = $C_6H_2\text{-}2,4,6\text{-}i\text{-}Pr_3$). *Organometallics* **1999**, *18* (4), 697−700.
(47) Niemeyer, M. A Tetranuclear Copper Compound Containing Three Different Types of Anions: *trans*-(μ-*tert*-butoxy)bis(μ-2,4,6,2',4',6'-hexamethyl-1,1':3',1'-terphenyl-2',2'-diyl)(μ-iodo)-tetracopper(I). *Acta Crystallogr., Sect. E: Struct. Rep. Online* **2001**, *57* (9), m416−m418.
(48) Niemeyer, M. Reaction of Copper Aryls with Imidazol-2-Ylidines or Triphenylphosphane - Formation of 1:1-Adducts with Two-Coordinate Copper Atoms. *Z. Anorg. Allg. Chem.* **2003**, *629* (9), 1535−1540.
(49) Hwang, C.-S.; Power, P. P. Synthesis and Characterization of $(THF)_3Li(NC)Cu(C_6H_3\text{-}2,6\text{-}Mes_2)$. *Bull. Korean Chem. Soc.* **2003**, *24* (5), 605−609.
(50) Niemeyer, M. An Unusual Ambivalent Tin(II)-Oxo Cluster. *Z. Anorg. Allg. Chem.* **2004**, *630* (2), 252−256.
(51) Hwang, C.-S.; Power, P. P. Synthesis and Characterization of the Lithium Organoargentate Salts $[Li(THF)_4][Ag(Triph)_2]{\cdot}THF$ and $[Li(THF)_4][Ag(C_6H_3\text{-}2,6\text{-}Mes_2)_2]{\cdot}1/8OEt_2$ (Triph = $-C_6H_2\text{-}2,4,6\text{-}Ph_3$; Mes = $C_6H_2\text{-}2,4,6\text{-}Me_3$). *J. Organomet. Chem.* **1999**, *589* (2), 234−238.
(52) Rabe, G. W.; Mitzel, N. W. Synthesis and X-Ray Crystal Structure Determination of the First Structurally Authenticated Terphenyl Gold Complex. *Inorg. Chim. Acta* **2001**, *316* (1−2), 132−134.
(53) Stollenz, M.; Taher, D.; Bhuvanesh, N.; Reibenspies, J. H.; Baranová, Z.; Gladysz, J. A. Steric Control of the in/out Sense of Bridgehead Substituents in Macrobicyclic Compounds: Isolation of New "Crossed Chain" Variants of in/out Isomers. *Chem. Commun.* **2015**, *51* (89), 16053−16056.
(54) Bader, R. F. W. *Atoms in Molecules: A Quantum Theory*, 2nd ed.; Clarendon Press, 1994.
(55) Bader, R. F. W. A Quantum Theory of Molecular Structure and Its Applications. *Chem. Rev.* **1991**, *91* (5), 893−928.
(56) Mitoraj, M.; Michalak, A. Natural Orbitals for Chemical Valence as Descriptors of Chemical Bonding in Transition Metal Complexes. *J. Mol. Model.* **2007**, *13*, 347−355.
(57) Michalak, A.; Mitoraj, M.; Ziegler, T. Bond Orbitals from Chemical Valence Theory. *J. Phys. Chem. A* **2008**, *112*, 1933−1939.
(58) Mitoraj, M. P.; Michalak, A.; Ziegler, T. A Combined Charge and Energy Decomposition Scheme for Bond Analysis. *J. Chem. Theory Comput.* **2009**, *5*, 962−975.
(59) Mitoraj, M. P.; Michalak, A. σ-Donor and π-Acceptor Properties of Phosphorus Ligands: An Insight from the Natural Orbitals for Chemical Valence. *Inorg. Chem.* **2010**, *49*, 578−582.
(60) Sharpe, H. R.; Geer, A. M.; Taylor, L. J.; Gridley, B. M.; Blundell, T. J.; Blake, A. J.; Davies, E. S.; Lewis, W.; McMaster, J.; Robinson, D.; Kays, D. L. Selective Reduction and Homologation of Carbon Monoxide by Organometallic Iron Complexes. *Nat. Commun.* **2018**, *9* (1), 3757.
(61) Roy, M. M. D.; Ferguson, M. J.; McDonald, R.; Rivard, E. Approaching Monocoordination at a Silver(I) Cation. *Chem. Commun.* **2018**, *54*, 483−486.
(62) Nguyen, T.; Merrill, W. A.; Ni, C.; Lei, H.; Fettinger, J. C.; Ellis, B. D.; Long, G. J.; Brynda, M.; Power, P. P. Synthesis and Characterization of the Metal(I) Dimers [Ar'MMAr']: Comparisons with Quintuple-Bonded [Ar'CrCrAr']. *Angew. Chem., Int. Ed.* **2008**, *47*, 9115−9117.

https://doi.org/10.1021/acs.inorgchem.0c03623
Inorg. Chem. 2021, 60, 10114−10123

(63) Lingnau, R.; Strähle, J. 2,4,6-$Ph_3C_6H_2M$ (M = Cu, Ag), Monomeric Cu^I- and Ag^I-Complexes with Coordination Number 1. *Angew. Chem., Int. Ed. Engl.* **1988**, *27* (3), 436.
(64) Haaland, A.; Rypdal, K.; Verne, H. P.; Scherer, W.; Thiel, W. R. The Crystal Structures of Base-Free, Monomeric Arylcopper(I) and Arylsilver(I) Compounds; Two Cases of Mistaken Identity? *Angew. Chem., Int. Ed. Engl.* **1995**, *33* (23−24), 2443−2445.
(65) Sapsford, K. E.; Algar, W. R.; Berti, L.; Gemmill, K. B.; Casey, B. J.; Oh, E.; Stewart, M. H.; Medintz, I. L. Functionalizing Nanoparticles with Biological Molecules: Developing Chemistries That Facilitate Nanotechnology. *Chem. Rev.* **2013**, *113* (3), 1904−2074.
(66) Grimme, S.; Brandenburg, J. G.; Bannwarth, C.; Hansen, A. Consistent Structures and Interactions by Density Functional Theory with Small Atomic Orbital Basis Sets. *J. Chem. Phys.* **2015**, *143* (5), 054107.
(67) Neese, F. The ORCA Program System. *Wiley Interdiscip. Rev.: Comput. Mol. Sci.* **2012**, *2* (1), 73−78.
(68) Neese, F. Software Update: The ORCA Program System, Version 4.0. *Wiley Interdiscip. Rev.: Comput. Mol. Sci.* **2018**, *8* (1), No. e1327.
(69) El-Bahraoui, J.; Dobado, J. A.; Molina, J. M. Metal-Metal Closed-Shell Interaction in M_2X_2 (M = Ag, Cu; X = Cl, Br, I) and Related Compounds $[Ag_2Br_2](PH_3)_3$ and $[Cu_2Cl_2](PH_3)_2$: An RHF, MP2 and DFT Study. *J. Mol. Struct.: THEOCHEM* **1999**, *493* (1−3), 249−257.
(70) Colacio, E.; Lloret, F.; Kivekäs, R.; Suárez-Varela, J.; Sundberg, M. R.; Uggla, R. Aurophilicity-Coordination Interplay in the Design of Cyano-Bridged Nickel(II)-Gold(I) Bimetallic Assemblies: Structural and Computational Studies of the Gold(I)-Gold(I) Interactions. *Inorg. Chem.* **2003**, *42* (2), 560−565.
(71) Dinda, S.; Samuelson, A. G. The Nature of Bond Critical Points in Dinuclear Copper(I) Complexes. *Chem. - Eur. J.* **2012**, *18* (10), 3032−3042.
(72) Mukherjee, G.; Singh, P.; Ganguri, C.; Sharma, S.; Singh, H. B.; Goel, N.; Singh, U. P.; Butcher, R. J. Selenadiazolopyridine: A Synthon for Supramolecular Assembly and Complexes with Metallophilic Interactions. *Inorg. Chem.* **2012**, *51* (15), 8128−8140.
(73) Koskinen, L.; Jääskeläinen, S.; Kalenius, E.; Hirva, P.; Haukka, M. Role of C-H···Au and Aurophilic Supramolecular Interactions in Gold-Thione Complexes. *Cryst. Growth Des.* **2014**, *14* (4), 1989−1997.
(74) Koskinen, L.; Jääskeläinen, S.; Hirva, P.; Haukka, M. Inter- and Intramolecular Non-Covalent Interactions in 1-Methylimidazole-2-Carbaldehyde Complexes of Copper, Silver, and Gold. *Solid State Sci.* **2014**, *35*, 81−87.
(75) Hapka, M.; Dranka, M.; Orłowska, K.; Chałasiński, G.; Szczêsniak, M. M.; Zachara, J. Noncovalent Interactions Determine the Conformation of Aurophilic Complexes with 2-mercapto-4-methyl-5-thiazoleacetic acid ligands. *Dalton Trans.* **2015**, *44* (30), 13641−13650.
(76) Estevan, F.; Hirva, P.; Ofori, A.; Sanaú, M.; Špec, T.; Úbeda, M. Pyrazole and Pyrazolate as Ligands in the Synthesis and Stabilization of New Palladium(II) and (III) Compounds. *Inorg. Chem.* **2016**, *55* (5), 2101−2113.
(77) Lu, T.; Chen, F. Multiwfn: A Multifunctional Wavefunction Analyzer. *J. Comput. Chem.* **2012**, *33* (5), 580−592.
(78) Lepetit, C.; Fau, P.; Fajerwerg, K.; Kahn, M. L.; Silvi, B. Topological Analysis of the Metal-Metal Bond: A Tutorial Review. *Coord. Chem. Rev.* **2017**, *345*, 150−181.
(79) Gervasio, G.; Bianchi, R.; Marabello, D. About the Topological Classification of the Metal-Metal Bond. *Chem. Phys. Lett.* **2004**, *387* (4−6), 481−484.
(80) Espinosa, E.; Alkorta, I.; Elguero, J.; Molins, E. From Weak to Strong Interactions: A Comprehensive Analysis of the Topological and Energetic Properties of the Electron Density Distribution Involving X-H···F-Y Systems. *J. Chem. Phys.* **2002**, *117* (12), 5529−5542.
(81) Espinosa, E.; Molins, E.; Lecomte, C. Hydrogen Bond Strengths Revealed by Topological Analyses of Experimentally Observed Electron Densities. *Chem. Phys. Lett.* **1998**, *285* (3−4), 170−173.
(82) Fradera, X.; Austen, M. A.; Bader, R. F. W. The Lewis Model and Beyond. *J. Phys. Chem. A* **1999**, *103* (2), 304−314.
(83) Outeiral, C.; Vincent, M. A.; Martín Pendás, Á.; Popelier, P. L. A. Revitalizing the Concept of Bond Order through Delocalization Measures in Real Space. *Chem. Sci.* **2018**, *9* (25), 5517−5529.
(84) Mayer, I. Charge, Bond Order and Valence in the AB Initio SCF Theory. *Chem. Phys. Lett.* **1983**, *97* (3), 270−274.
(85) N.B.: In the *ORCA 4.0.1* implementation of EDA-NOCV, the electrostatic and Pauli terms cannot be separated.
(86) Hanwell, M. D.; Curtis, D. E.; Lonie, D. C.; Vandermeersch, T.; Zurek, E.; Hutchison, G. R. Avogadro: An Advanced Semantic Chemical Editor, Visualization, and Analysis Platform. *J. Cheminf.* **2012**, *4*, 17.
(87) Baya, M.; Belío, Ú.; Fernández, I.; Fuertes, S.; Martín, A. Unusual Metal-Metal Bonding in a Dinuclear Pt-Au Complex: Snapshot of a Transmetalation Process. *Angew. Chem., Int. Ed.* **2016**, *55*, 6978−6982.
(88) Oeschger, R. J.; Chen, P. Structure and Gas-Phase Thermochemistry of a Pd/Cu Complex: Studies on a Model for Transmetalation Transition States. *J. Am. Chem. Soc.* **2017**, *139* (3), 1069−1072.
(89) Paenurk, E.; Gershoni-Poranne, R.; Chen, P. Trends in Metallophilic Bonding in Pd-Zn and Pd-Cu Complexes. *Organometallics* **2017**, *36* (24), 4854−4863.
(90) Oeschger, R. J.; Chen, P. A Heterobimetallic Pd-Zn Complex: Study of a d^8-d^{10} Bond in Solid State, in Solution, and in Silico. *Organometallics* **2017**, *36* (8), 1465−1468.
(91) Pyykkö, P.; Zhao, Y. Ab Initio Calculations on the $(ClAuPH_3)_2$ Dimer with Relativistic Pseudopotential: Is the "Aurophilic Attraction" a Correlation Effect? *Angew. Chem., Int. Ed. Engl.* **1991**, *30*, 604−605.
(92) Pyykkö, P.; Li, J.; Runeberg, N. Predicted Ligand Dependence of the Au(I)···Au(I) Attraction in $(XAuPH_3)_2$. *Chem. Phys. Lett.* **1994**, *218*, 133−138.
(93) Magnko, L.; Schweizer, M.; Rauhut, G.; Schütz, M.; Stoll, H.; Werner, H.-J. A Comparison of Metallophilic Attraction in $(X\text{-}MPH_3)_2$ (M = Cu, Ag, Au; X = H, Cl). *Phys. Chem. Chem. Phys.* **2002**, *4*, 1006−1013.
(94) O'Grady, E.; Kaltsoyannis, N. Does Metallophilicity Increase or Decrease down Group 11? Computational Investigations of $[Cl\text{-}MPH_3]_2$ (M = Cu, Ag, Au, [111]). *Phys. Chem. Chem. Phys.* **2004**, *6*, 680−687.
(95) Brandys, M. C.; Jennings, M. C.; Puddephatt, R. J. Luminescent Gold(I) Macrocycles with Diphosphine and 4,4'-Bipyridyl Ligands. *J. Chem. Soc., Dalton Trans.* **2000**, 4601−4606.

https://doi.org/10.1021/acs.inorgchem.0c03623
Inorg. Chem. 2021, 60, 10114−10123